# Theory of Dissociative Recombination of $D_{3h}$ Triatomic Ions Applied to $H_3^+$

Viatcheslav Kokoouline and Chris H. Greene

*Department of Physics and JILA, University of Colorado, Boulder, Colorado 80309-0440*

(Received 3 December 2002; published 3 April 2003)

We propose a fully quantal description of $H_3^+$ dissociative recombination. The new method combines multichannel quantum defect theory, the adiabatic hyperspherical approach, and the techniques of outgoing-wave Siegert pseudostates. The vibrational, rotational, nuclear spin degrees of freedom of the ion, in their full dimensionality, are all taken into account for the first time in any calculation of polyatomic dissociative recombination. Our calculation of the recombination rate confirms that the Jahn-Teller effect is responsible for the large rate in $H_3^+$. The resulting theoretical rates for dissociative recombination of $H_3^+$ are in good general agreement with experiment.

DOI: 10.1103/PhysRevLett.90.133201 PACS numbers: 34.80.Ht, 34.80.Kw, 34.80.Lx

The dissociative recombination (DR) of $H_3^+$ ions is a fundamental process in diffuse interstellar clouds. It is also the simplest triatomic ion and for this reason its theoretical description can serve as a prototype for other polyatomic ions. Meanwhile, experimental determinations of the recombination rate vary widely, which has resulted in some controversy and confusion [1]. Until recently, it has seemed unlikely that this problem could be resolved by theoretical studies, because the mechanism of $H_3^+$ DR was still not known. In a recent study [2], we presented evidence that the inclusion of Jahn-Teller coupling can produce a DR rate that overlaps the range of experimental observations. The goal of the present study is to present a fully quantum theoretical method that can describe DR in $H_3^+$ and other triatomic molecules, including the full, three-dimensional motion of the rotating, vibrating, and dissociating nuclei.

In this Letter, we address a number of problems that have hindered a full description of DR in $H_3^+$ until now: (i) In contrast to diatomics, the vibrational degrees of freedom have three dimensions. (ii) Symmetry-breaking Jahn-Teller effects have not previously been treated, despite evidence of their importance from $H_3$ photoabsorption studies. (iii) The lone dissociative electronic surfaces of $H_3$ that are energetically accessible at low energy fail to cross the ground state ionic potential surface, which was believed in the past to result in very low DR rates. Such molecules require a theoretical method that can correctly describe indirect recombination via intermediate Rydberg state pathways. (iv) The multichannel quantum defect theory (MQDT) description of complicated molecular Rydberg state interactions has been applied to treat the dissociation of diatomic molecules [3,4], but it has not yet been able to describe dissociative channels for triatomics. (v) The rotational degrees of freedom, rarely included in DR calculations, even for diatomics, could play a significant role in $H_3^+$. This is because DR is thought to hinge on the time reverse of autoionization, i.e., on the capture of an incident electron into a Rydberg state, and because rotational autoionization generates the broadest autoionization widths observed until now in $H_3$ Rydberg states.

Our approach to deal with these five problems combines theoretical elements that have not previously been unified. To be specific, quantum defect theory is employed to describe the electron-ion scattering at a fixed nuclear configuration. The quantum defect parameters include Jahn-Teller coupling physics, extracted from *ab initio* $H_3$ Rydberg state surfaces. The electron scattering amplitude from one rovibrational ionic level to another is constructed using rotational and vibrational frame transformation techniques [4]. The resulting scattering matrix has ionization channel indices only, but is nonunitary, which reflects the possibility for dissociative fragmentation. The dissociation happens following an initial capture into a rovibrationally excited Rydberg state [5]. Another key improvement in the present work has been the elimination of a previously unrecognized inconsistency between the $K$-matrix convention of Ref. [6] and that adopted in Refs. [7–9] and later by Ref. [2]. Specifically, the right-hand side of Eq. (4) of Ref. [2] must be multiplied by $-\pi$ in order to correct that inconsistency. Roughly speaking, this increases both the lower and upper bounds to the DR rates presented in Ref. [2] by approximately $\pi^2$, and is the single most important reason why the DR rate presented in this paper exceeds the "theoretical upper bound" presented in that work.

The molecular symmetry group of $H_3^+$ is $D_{3h}(M)$ [10]. Every group operation $\mathcal{O}$ can be represented as a product of three operations: nuclear spin permutation, rotation of the molecular frame, and permutation of spatial displacements of nuclei from the symmetric configuration. Correspondingly, the total wave function $\Phi_t^{\text{n.sym}}$ of the ion can be represented as a product of nuclear spin, rotational, and vibrational terms:

$$\Phi_t^{\text{n.sym}} = \Phi_I \mathcal{R}^{N^+}_{m^+,K^+}(\alpha\beta\gamma)\mathcal{V}(v_1, v_2^{l_2}; \mathcal{Q}). \qquad (1)$$

In the equation, $\alpha$, $\beta$, $\gamma$ are three Euler angles defining the orientation of the molecular fixed coordinate system (MS)

  

with respect to the laboratory fixed coordinates system (LS). $\mathcal{Q}$ is the triad of coordinates describing internuclear distances. We use three hyperspherical coordinates to represent $\mathcal{Q}$. The total nuclear spin is $I = 1/2$ (para) or $3/2$ (ortho). The rotational part $\mathcal{R}^{N^+}_{m^+,K^+}(\alpha\beta\gamma)$ of the wave function in Eq. (1) is the symmetric top eigenfunction, which is proportional to the Wigner function [10]. Vibrational wave functions $\mathcal{V}(v_1, v_2^{l_2}; \mathcal{Q})$ of the ion depend on three coordinates $\mathcal{Q}$, which are specified by the triad of quantum numbers $(v_1, v_2^{l_2})$ [11]. The nuclear spin kets are constructed to transform according to $A_1$ or $E_\pm = (E_a \pm iE_b)/\sqrt{2}$ irreducible representations of the permutation group $S_3$ of three identical particles. Representations $E_a$ and $E_b$ comprise the degenerate two-dimensional $E$ representation of $S_3$ [10].

To obtain the ionic wave function that transforms properly under the symmetry operations of $D_{3h}(M)$, we construct antisymmetric combinations in a spirit described by Watson [11]. One difference with the Watson formula is that we have also included antisymmetrization of the nuclear spins, in order to account for the ortho and para forms of $H_3^+$:

$$\Phi_{\text{tot}} = \frac{1}{\sqrt{2}}[\Phi_t^{\text{n.sym}}(K^+, l_2, g_I) - (-1)^{N^+ + l_2}\Phi_t^{\text{n.sym}}(-K^+, -l_2, -g_I)], \quad (2)$$

where the quantum number $g_I$ determines the transformations of the nuclear part of the total wave function under the (123) operation. $g_I = 0$ for $A_1$ ($I = 3/2$) and $g_I = 1$ or $g_I = -1$ for $E_+$ or $E_-$ ($I = 1/2$). The Pauli principle implies that $\Phi_{\text{tot}}$ should transform according to the $A_2'$ or $A_2''$ representations of the $D_{3h}(M)$ group. This is true if $G = 0 \bmod 3$, where $G = K^+ + l_2 + g_I$. The total parity of the ionic state is $(-1)^{K+}$. The symmetry of the $e^- + H_3^+$ complex is determined by symmetries of the ion and the electron. The electron wave function $Y_{1\lambda}$ attached to the wave function of Eq. (1) affects only the total parity, contributing a factor $(-)^l$. To specify ionic states, we will use the notation $\Gamma(v_1, v_2, ^{l_2})\{N^+, K^+\}^{(s)}$, where $(s)$ will be $(o)$ or $(p)$ relating to $I = 3/2$ or $I = 1/2$, $\Gamma$ is the total ionic symmetry, $A_1'$ or $A_1''$.

To treat the vibrational dynamics in three dimensions, we employ the adiabatic hyperspherical approach in two steps. First, we determine the adiabatic hyperspherical potential curves $U_i^+(R)$ and adiabatic eigenfunctions $\Phi_{v_2 l_2}(R; \Omega)$ as parametric functions of the hyper-radius $R$. This requires solution of a two-dimensional partial differential equation in the two hyperangles [12]. Second, we solve a one-dimension radial Schrödinger equation in each such potential curve, for a truncated set of vibrational states $\mathcal{F}(v_1, v_2^{l_2})$ and eigenenergies $E_{v_1, v_2^{l_2}}$. The products $\Phi\mathcal{F}$ give a good approximation to the actual vibrational eigenstates $\mathcal{V}(v_1, v_2^{l_2}; \mathcal{Q})$ of the ion. In fact, the hyper-radial ionic wave functions are chosen to obey outgoing-wave, Siegert boundary conditions at the boundary of a finite box, within $R < R_0$. However, the vibrational continuum is discretized with Siegert pseudostates [13,14] having complex eigenenergies, a subset of which we retain that are outgoing waves at the boundary. These Siegert pseudostates are introduced to let the dissociative flux escape if it reaches the hyper-radial boundary, through the procedures introduced in [14]. Every Siegert pseudostate of every ionic potential curve generates a Rydberg series of neutral states. Once the vibrational states are calculated, the scattering matrix describing the collision of the electron with the vibrating $H_3^+$ ion is constructed through the rovibrational frame transformations [15]. Because of the presence of Siegert states with complex eigenenergies, this electron-ion scattering matrix is not unitary. The nonunitarity accounts for the fact that the electron can get stuck in a Rydberg state with excited ionic vibration, leading to an enhanced probability for dissociation of the system into neutral products.

The states at large electron-ion separations can be accurately represented as coupled product solutions $[\mathcal{R}^{N^+}_{K^+}(\alpha\beta\gamma)Y^l(\theta, \varphi)]^{(N)}\mathcal{V}(v_1, v_2^{l_2})$ (Hund's case $d$), where $\theta, \varphi$ are spherical angles of the electron in LS. At small electron-ion separations, the suitable wave functions are the Hund's case $b$ combinations $\mathcal{R}^N_{m,K}(\alpha\beta\gamma)Y_{l\Lambda}(\theta', \varphi')|\mathcal{Q}\rangle$, where $\theta', \varphi'$ determines now the position of the electron in respect to MS, and $\Lambda$ is the projection of electron angular momentum on the molecular axis. The unitary transformation matrix between the two sets is given by $\langle N^+K^+|\Lambda K\rangle^{(lN)} = (-1)^{1-\Lambda}C^{N^+,K^+}_{l,-\Lambda;N,K}$. The superscript $(N)$ means that angular momenta $N^+$ and $l$ are coupled to give a definite value of $N$. Specification of $N$ is permissible since it is a good quantum number in both representations.

The total scattering matrix is constructed using the techniques of the frame transformation: When the electron is far from the ion, the Hund's case $d$ wave functions diagonalize the interaction Hamiltonian; at short distances, Hund's case $b$ wave functions almost diagonalize the Hamiltonian. The short-range Hamiltonian has off-diagonal elements in $\Lambda$ that reflect Jahn-Teller coupling. The following selection rules can be formulated: (i) The Hamiltonian couples only vibrational states of the same vibrational symmetry, and the same value of $\Lambda$, or (ii) it can couple the rovibrational channels according to the rule $(\Lambda = 1, l_2 = -1) \leftrightarrow (\Lambda' = -1, l_2' = 1)$. These selection rules ensure that the parity of the system and the quantum number $G$ related to the total rovibrational angular momentum are conserved during the collision. The actual form of the coupling matrix as a function of the normal coordinates was presented in [6,8,9], though it must be corrected for the missing factor of $-\pi$ mentioned above. We give only the expression for the full scattering matrix, in a representation that is not yet symmetrized:

$$S^{N,K,\pi}_{i';i} = \sum_{\Lambda,\Lambda',K^+,K^{+\prime}} C^{N^{+\prime},K^{+\prime}}_{l,-\Lambda';N,K}\left[\int_s \mathcal{V}(v'_1, v'^{l'_2}_2; \mathcal{Q}) S_{\Lambda,\Lambda'}(\mathcal{Q}) \mathcal{V}(v_1, v^{l_2}_2; \mathcal{Q}) d\mathcal{Q}\right] C^{N^+,K^+}_{l,-\Lambda;N,K}(-1)^{\Lambda+\Lambda'}. \quad (3)$$

where $i \equiv \{N^+, K^+, v_1, v^{l_2}_2\}$. The integral $\int_s$ in the above equation is the usual integral over vibrational coordinates if either vibrational function vanishes at $R = R_0$. For states nonzero at $R_0$, the integral has an additional surface term describing the possibility for vibrational flux to escape from the interaction zone [14]. The last step in construction of the total scattering matrix is the symmetrization procedure of Eq. (2), which is applied after the rovibrational frame transformation. Equation (3) does not yet specify the total molecular symmetry $\Gamma = A'_2$ or $A''_2$ of the collision complex, nor the total spin $I = \frac{1}{2}$ or $\frac{3}{2}$. These are conserved during the collision. Therefore, the cross section can be calculated separately for all four resulting total symmetries. The resonance positions in the MQDT calculation are highly sensitive to the ion excitation energies. Accordingly, we use very accurate levels available in the literature [16].

The scattering matrix $S$ obtained above is the so-called short-range $S$ matrix that includes amplitudes for an electron to scatter into a closed rovibrational channel whose ionic energy exceeds the total energy of the system. The physical long-range matrix $S^{\text{phys}}(E)$ is obtained by the standard MQDT "closed channel elimination" procedure [see formula (2.50) of Ref. [17]]. The matrix $S^{\text{phys}}(E)$ has $N_o \times N_o$ dimension, where $N_o$ is the number of open channels at energy $E$. For calculation of the cross section, we need also the conjugated scattering matrix. Owing to the properties of the Siegert vibrational states utilized, the conjugated scattering matrix $S^{\dagger\text{phys}}(E)$ is not just the Hermitian conjugate of the scattering matrix $S^{\text{phys}}(E)$. Therefore, the conjugated matrix $S^{\dagger\text{phys}}(E)$ is obtained in a separate MQDT calculation; the only differences being that, at the outset, the conjugated $S^{\dagger}_{\Lambda,\Lambda'}(\mathcal{Q})$ is used instead of $S_{\Lambda,\Lambda'}(\mathcal{Q})$, and the sign of $\beta = \pi\nu$ is reversed.

Using the separately calculated matrices $S^{\text{phys}}(E)$ and $S^{\dagger\text{phys}}(E)$, for each incident channel $i'$ the probability for dissociative recombination is calculated using the "defect" from unit normalization of that column of the scattering matrix:

$$\mathcal{P}(\mathcal{E}) = 1 - \sum_{i=1,N_o} S^{\text{phys}}_{i'i}(E)[S^{\dagger}]^{\text{phys}}_{ii'}(E), \quad (4)$$

where $i'$ is the electron entrance channel. In the storage-ring experiments, the entrance channel is always the ground vibrational ionic state, but the rotational quantum number can vary: $i' = \{0, 0^0\}(N^+, K^+)$. Since the scattering process conserves the total symmetry ($\Gamma = A'_2$ or $A''_2$) of the ion and the total nuclear momentum $I = 1/2$ or $3/2$, the cross sections for all four combinations $\Gamma^+, I$ are calculated separately. As was suggested in Ref. [14], convergence of the Siegert expansion was monitored with care.

Figure 1 shows the calculated rate (dashed and solid lines) as a function of the relative electron energy $E_\parallel$ ($E_\parallel$ is the longitudinal energy component) compared with data from two storage-ring experiments—triangles [18] and circles [19]. The calculated rate coefficient has been averaged over an energy spread $\bar{E}_\perp$, and over the ionic rotational temperature $kT_{\text{rot}}$. The solid curve is calculated using 6 meV resolution in $\bar{E}_\perp$, and should be compared with the corresponding data (triangles) [18]. The dashed calculated line should be compared with data from Ref. [19] (circles).

The first thing that stands out in the comparison between theory and experiment is that, for the first time, theory is in generally the same magnitude as experiment over most energies of the figure. In some regions, e.g., around 0.1 and 0.4 eV, the theoretical rate is significantly lower than the measured rate. This disagreement is not yet understood, but one possibility is that some higher rotational levels may still be present in the storage-ring experiments. Our calculations for excited rotational states of the ion show that this gap tends to be filled up if the next rotational states are included in our calculation. The rotational temperature of $H_3^+$ in the storage-ring experiment by Jensen *et al.* [19] may be as high as 2700 K. Our calculation at $T_{\text{rot}} = 600$ K (the highest $T_{\text{rot}}$ we can treat

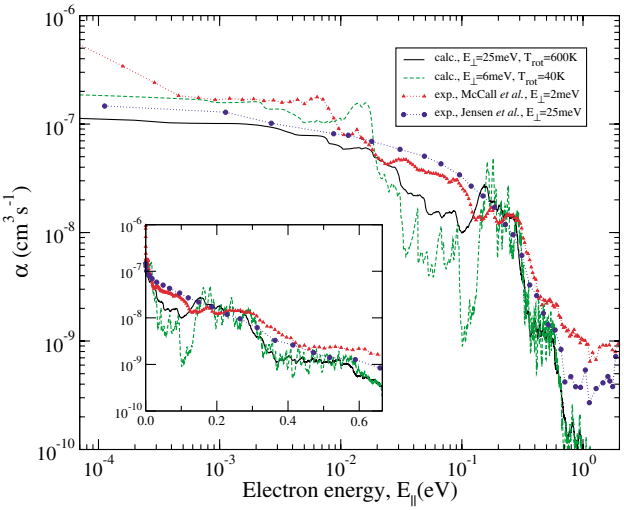


FIG. 1 (color online). Comparison of calculated and experimental rates of dissociative recombination. The calculated rate (solid and dashed lines) is shown as a function of the (parallel) electron energy. In the theoretical curves, the rate has been thermally averaged over the lowest rotational states, using a 40 K rotational temperature. Theoretical curves are shown for two different values of the transverse energy spread, $\bar{E}_\perp =$ 6 meV (dashed curve) and 25 meV (solid curve). The experiments are shown: McCall *et al.* [18] at $\bar{E}_\perp = 2$ meV as triangles, and Jensen *et al.* [19] at $\bar{E}_\perp = 25$ meV as circles.

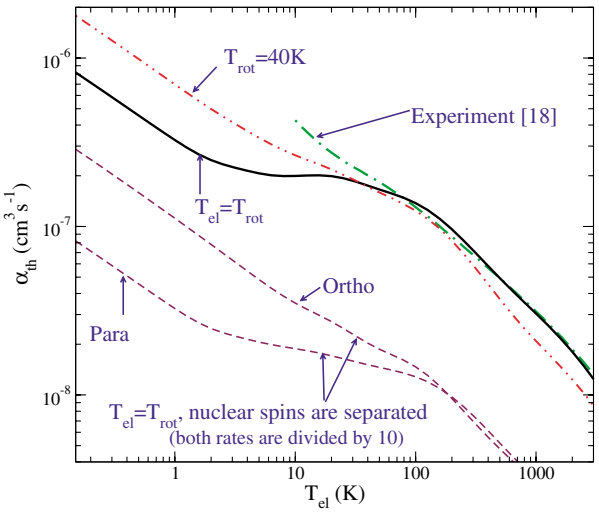


FIG. 2 (color online). The theoretical thermally averaged recombination rate (solid line) is shown as a function of temperature. This curve is the one most relevant to compare with astrophysical observations of $H_3^+$. The theoretical curve manifests a plateaulike behavior, which differs from the new experimental results (dot-dashed curve) [18] at low temperatures. The thick dash-dotted curve represents the experimentally extracted thermal rate [18], which can be compared with our double-dot-dashed curve calculated for their stated ion source conditions.

using only eight rotational levels), shows better agreement with the Ref. [19] experiment, shown in Fig. 1. In the experiment of Ref. [19], the initial rotational temperature of ions is measured to be much lower (20–60 K), but it does not show the dip between 0.035 and 0.1 eV. The experimental curve with high rotational temperature shows virtually no resonances, whereas the experimental curve at low rotational temperature shows some resonances, but far fewer than we predict.

The reason why stationary afterglow experiments [20] measure a low DR rate so much smaller than the results in Fig. 2 remains a mystery. In view of the presence of perturbing species in the vicinity of the recombining ions, and in view of the vital role of easily affected Rydberg state pathways, it seems plausible that these controlling contributions might be modified in an afterglow experiment. A detailed model of pressure or field effects on those pathways remains a desirable goal for future investigations. Another flowing-afterglow experiment [21] gives a rate coefficient $\alpha(300\ \mathrm{K}) = 7.8 \pm 2.3 \times 10^{-8}\ \mathrm{cm}^3/\mathrm{s}$ which is consistent with our calculated rate $\alpha_{\mathrm{th}}(300\ \mathrm{K}) = 7.2 \pm 1.1 \times 10^{-8}\ \mathrm{cm}^3/\mathrm{s}$. Space limitations allow us to mention only briefly that the DR rate for $D_3^+$ is calculated to be lower than that for $H_3^+$ by approximately a factor of 3 at 300 K. This is in approximate agreement with the $D_3^+$ storage-ring experiment [22].

In conclusion, we have developed a new theoretical treatment capable of describing nonperturbative dissociative recombination processes in low energy collisions with triatomic ions. It accounts theoretically for many aspects of the $H_3^+$ storage-ring experiment. An accurate theoretical description of the rate coefficient measured in storage-ring experiments has been obtained for the first time, for this simplest of all polyatomic molecules.

This work has been supported in part by NSF, by the DOE Office of Science, and by an allocation of NERSC supercomputing resources. The authors are grateful to A. Dalgarno, G. Dunn, J. Hutson, M. Larsson, B. McCall, T. Oka, and J. Stephens for fruitful discussions and to E. Hamilton and B. Esry for assistance.

[1] M. Larsson, Philos. Trans. R. Soc. London A **358**, 2433 (2000).
[2] V. Kokoouline, C. H. Greene, and B. D. Esry, Nature (London) **412**, 891 (2001).
[3] A. Matzkin, Ch. Jungen, and S. C. Ross, Phys. Rev. A **62**, 062511 (2000).
[4] Ch. Jungen, *Molecular Applications of Quantum Defect Theory* (Institute of Physics, Bristol, 1996).
[5] I. F. Schneider, A. E. Orel, and A. Suzor-Weiner, Phys. Rev. Lett. **85**, 3785 (2000).
[6] A. Staib and W. Domcke, Z. Phys. D **16**, 275 (1990).
[7] J. A. Stephens and C. H. Greene, Phys. Rev. Lett. **72**, 1624 (1994).
[8] J. A. Stephens and C. H. Greene, J. Chem. Phys. **102**, 1579 (1995).
[9] I. Mistrík, R. Reichle, U. Muller, H. Helm, M. Jungen, and J. A. Stephens, Phys. Rev. A **61**, 033410 (2000).
[10] P. Bunker and P. Jensen, *Molecular Symmetry and Spectroscopy* (NRC Research Press, Ottawa, 1998).
[11] J. K. G. Watson, Philos. Trans. R. Soc. London A **358**, 2371 (2000).
[12] B. D. Esry, C. D. Lin, and C. H. Greene, Phys. Rev. A **54**, 394 (1996).
[13] O. I. Tolstikhin, V. N. Ostrovsky, and H. Nakamura, Phys. Rev. A **58**, 2077 (1998).
[14] E. L. Hamilton and C. H. Greene, Phys. Rev. Lett. **89**, 263003 (2002).
[15] C. H. Greene and Ch. Jungen, Adv. At. Mol. Phys. **21**, 51 (1985).
[16] C. M. Lindsay and B. J. McCall, J. Molec. Spectr. **210**, 60 (2001).
[17] M. Aymar, C. H. Greene, and E. Luc-Koenig, Rev. Mod. Phys. **64**, 1015 (1996).
[18] B. J. McCall *et al.*, Nature (London) **422**, 500 (2003).
[19] M. J. Jensen, H. B. Pedersen, C. P. Safvan, K. Seiersen, X. Urbain, and L. H. Andersen, Phys. Rev. A **63**, 052701 (2001)
[20] J. Glosík, R. Plasil, V. Poterya, P. Kudrna, and M. Tichy, Chem. Phys. Lett. **331**, 209 (2000).
[21] S. Laubé, A. LePadellec, O. Sidko, C. Rebrion-Rowe, J. B. A. Mitchell, and B. R. Rowe, J. Phys. B **31**, 2111 (1998).
[22] M. Larsson, H. Danared, A. Larson, A. LePadellec, J. R. Peterson, S. Rosen, J. Semaniak, and C. Stromholm, Phys. Rev. Lett. **79**, 395 (1997).